PCCP

Accepted Manuscript

ROYAL SOCIETY OF CHEMISTRY

www.rsc.org/pccp

Journal Name Physical Chemistry Chemical Physics Dynamic Article Links ►

Cite this: DOI: 10.1039/c0xx00000x

www.rsc.org/xxxxxx

ARTICLE TYPE

The biocompatibility and anti-biofouling properties of magnetic core-multishell Fe@C NWs/AAO nanocomposites

André M. Lindo[a,b], Eva Pellicer[c], Muhammad A. Zeeshan[a], Roman Grisch[a], Famin Qiu[a], Jordi Sort[c,d], Mahmut S. Sakar[a], Bradley J. Nelson[a], Salvador Pané[a]

Received (in XXX, XXX) Xth XXXXXXXXX 20XX, Accepted Xth XXXXXXXXX 20XX
DOI: 10.1039/b000000x

Soft-magnetic core-multishell Fe@C NWs/AAO nanocomposites were synthesized using anodization, electrodeposition and low-pressure chemical vapour deposition (CVD) at 900 ºC. High chemical and mechanical stability is achieved by the conversion from amorphous to θ- and δ-Al_2O_3 phases above 600 ºC. Moreover, the surface properties of the material evolve from bioactive, for porous AAO, to bioinert, for Fe@C NW filled AAO nanocomposite. Although the latter is not cytotoxic, cells do not adhere onto the surface of the magnetic nanocomposite, thus proving its anti-biofouling character.

AAO-based nanocomposites, electrodeposition, ferromagnetism, surface polarity, biocompatible (bioinert), anti-biofouling

Introduction

Nanocomposites consisting of a matrix containing well-organized zero or one-dimensional nanostructures (nanoparticles, nanowires (NWs) or nanotubes) exhibit unique properties, which can be advantageous for several applications such as catalysis, data storage, magnetic actuation, optical sensing or biomedical implanting. The organization of nanostructures in matrices can be attained by suitable chemical procedures, or by producing or incorporating particles in pre-existing templates. For example, nanoscopic one-, two-, or three-dimensional arrangements of nanoparticles can be obtained using block copolymers-based supramolecules after solvent annealing.[1] Nanostructures can also be programmed to occupy spaces in arrays or templates. Maxit et al. have shown a facile method to selectively arrange ceria nanoparticles in the sheets of a polymer in a long-range ordered diblock polymer template.[2] Anodized aluminum oxide (AAO) templates have been also used to fabricate long-range ordered nanocomposites. Gösele and co-workers,[3] for instance, have fabricated a flow-through nanoporous gold nanowire/AAO composite membranes. The use of AAO arrays in the production of nanocomposites is advantageous in several aspects. First, AAO templates constitute mechanically robust platforms to grow materials that otherwise exhibit brittle fracture, such as metallic foams.[3] Also, AAO template nanochannels can present very high aspect ratios and wide pore-size tunability which is an outstanding feature when compared to conventional lithographic techniques. This is of particular interest, especially when anisotropic properties are desired in the composite. Furthermore, several techniques such as electrodeposition, sol-gel or capillary filling can be used to grow materials of different nature or combinations thereof in AAO channels. Besides, alumina is also regarded as bioinert material and therefore a good candidate for biomedical applications.[4] Alumina has more than 15 intermediate metastable crystallographic phases, including γ-, δ-, θ- and α-Al_2O_3 depending on the processing temperature.

AAO templates have been widely used as implantable platforms for biomedical applications[5] such as cell-interface studies, drug delivery, immunoisolation or biosensing. The advantage of using these membranes in biomedical devices is that they exhibit excellent chemical stability in the presence of biomolecules. Moreover, the surface of AAO can be chemically modified to change its surface polarity. This feature is particularly important, specially for devices in which cell adhesion must be enhanced, such as in cell culturing, or in which biofouling must be avoided, e.g. in sensing or drug delivery applications.[6]

Here, we present an ordered magnetic composite consisting of core-multishell iron-carbon NWs trapped in thermally treated AAO nanochannels. The fabrication flow is depicted in Fig. 1(a). These composites are produced by first anodizing a layer of aluminum (Al) previously deposited by e-beam evaporation onto a modified silicon substrate. NWs are subsequently electrodeposited within the channels of the AAO templates and afterwards a carbonaceous multishell is deposited conformally around the NWs by CVD. By taking advantage of the temperature conditions in which CVD takes place, it is possible to simultaneously change the quality of the carbon shells as well as the crystalline structure of the alumina, which in turn causes changes in the AAO chemical stability and its surface polarity.

This changes enable to create chemically stable magnetic nanocomposites for biomedical applications with anti-bioufouling attributes.

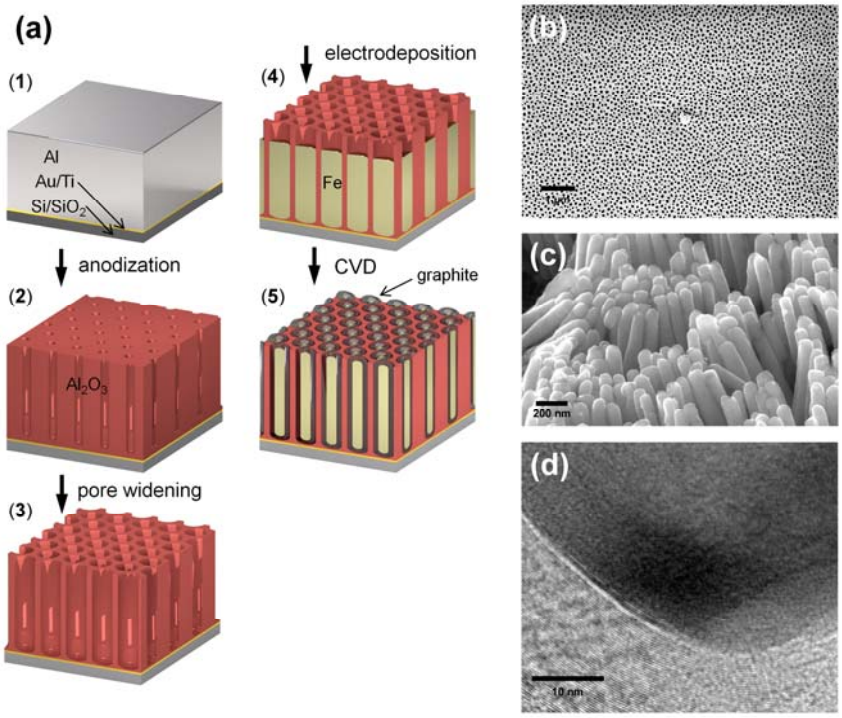

Fig. 1 (a) Fabrication steps to obtain the Fe@C NWs/AAO magnetic nanocomposite. (step 1.) A conductive layer (Au / Ti) and an Al layer are evaporated on the substrate (Si / SiO_2). (step 2.) Porous AAO is obtained after anodization of the Al layer. (step 3.) The pore diameter is widened and the barrier layer is thinned by etching. (step 4.) Fe is electrodeposited into the pores. (step 5.) The Fe NWs are coated with carbon by CVD. (b) SEM image of pore widened AAO templates obtained after step 3. (c) and (d) SEM and HRTEM images of carbon coated Fe NWs produced in step 5. at 750 ºC, after dissolving the AAO template.

Materials and Methods

Preparation of the Fe@C NWs / AAO nanocomposites: The essential steps of the nanocomposite fabrication were reported elsewhere.[7,8] Briefly, low-resistivity silicon wafers were used as substrates for the e-beam evaporation of 6 nm titanium (Ti), 12 nm gold (Au) and 1.5 μm Al layers. On the backside of these wafers an insulating layer of 1.5 μm silicon dioxide (SiO_2) was deposited. AAO templates were obtained by single step anodization on chips. This process was carried out in a two-electrode bath containing 0.3 M oxalic acid. The applied anodization potential was +60 V. The anodization was stopped when the measured current reached +200 mA. Enlargement of pore diameter and barrier layer thining was conducted in a 5.5 wt% phosphoric acid solution for 45 min. In order to fill the pores of the AAO templates with iron, pulsed electrodeposition (PED) was conducted using an electrolyte containing 0.2 M iron sulphate heptahydrate, 0.0028 M ascorbic acid and 0.1 M glycine (Sigma-Aldrich) at pH 4. To grow the carbonaceous coating on iron, a low pressure chemical vapour deposition process (LPCVD) was used. AAO templates filled with Fe NWs were placed on a heater inside a commercial CVD system (Black Magic, Aixtron Ltd). The temperature was increased at a ramp rate of 300 ºC/min under a H_2 / Ar flow of 160 and 240 sccm, respectively. The nitrogen flow was fixed at 80 sccm. The growth is achieved by adding a flow of 4 sccm acetylene (C_2H_2) for 5 min. The partial pressure ratio of C_2H_2 to H_2 was maintained at 1:40.

Characterization of the samples: The morphology of the samples was characterized using a scanning electron microscope (Zeiss ULTRA 55). The graphitic coating was observed with a transmission electron microscope (Philips CM12, 100kV) by dispersing the NW suspension on a 400 mesh copper grid with a ultrathin carbon layer on a holey carbon support film (Ted Pella Inc.). Raman spectra of the graphitic coating was obtained using a WITec CRM 200 spectrometer equipped with a 532 nm green laser at room temperature (RT). Cross-sections of the nanocomposite were prepared using a focused ion beam (FIB) with a milling current of 700 pA and imaged by SEM (Zeiss NVision 40). XRD was carried out on a Philips X'Pert diffractometer using Cu Kα radiation, with 0.03º step size and 10 s holding time. Magnetic hysteresis loops were obtained at room temperature by applying a maximum magnetic field of 1 T on C-coated and uncoated Fe NWs embedded in AAO templates using a vibrating sample magnetometer (Oxford Instruments VSM 1.2). To assess the wettability of the nanocomposites surface, the contact angle of Dulbecco's modified eagle medium (DMEM) with 10 % fetal bovine serum (FBS) drops (5 μL) deposited onto the surface was measured using a drop shape analyzer DSA 100

from KRÜSS at room temperature (static sessile drop technique).

Cytotoxity and Biocompatibility tests: 3T3 fibroblasts (ATCC, USA) were cultured in Dulbecco's minimal essential medium (MEM) with 10 % FBS and 1 % penicillin/streptomycin at 10 % CO_2 at 37 °C. The Fe@C NWs/AAO composites were washed by multiple immersions in ethanol and DI-water and subsequently sterilized with UV light. To evaluate the cytotoxicity, samples were submerged in culture medium in a 12-well plate. After 24 hours of incubation, the gel-conditioned medium was transferred to the cultured cells. Cells seeded in fresh media were used as a control. After incubation for 48 h, WST-1 reagent (Roche, Switzerland) was added to each well according to the manufacturer's instructions. Three hours later, 50 µL of the solution was transferred into a 96-well plate, and the absorbance was measured at 435 nm. Ten parallel experiments were performed for every sample. Absorbance values were obtained using a UV/VIS/NIR spectrometer. To assess the biocompatibility of the samples, the materials were tested for cell adhesion and proliferation. Cells were cultured on top of the samples for 48 hours in culture medium and cell density and morphology were visually characterized from images taken with an inverted fluorescence microscope (Olympus IX 81). The samples that showed cell proliferation were first immersed in 4% paraformaldehyde in phosphate buffer solution (PBS) for 1 h for chemical fixation. The fixed cells were then rinsed with fresh PBS and gradually dehydrated by immersing the sample in 10%, 25%, 50%, 75%, 90% and 100% ethanol, and each step maintained during 5 minutes. Next, the samples were dried by critical point drying (CPD 030, Bal-Tec) and a thin film of platinum (about 10 nm) was sputtered onto the sample as a conductive layer for SEM inspection (Zeiss ULTRA 55).

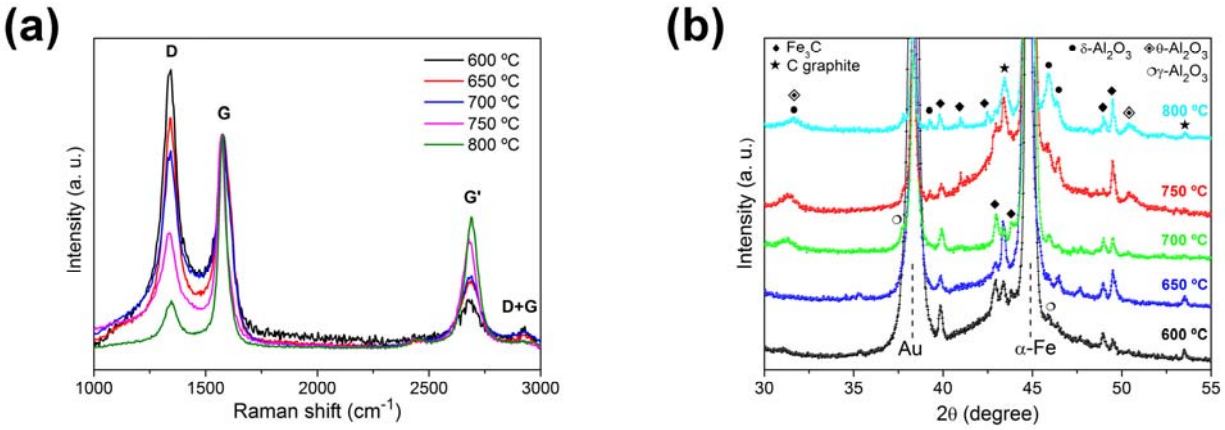

Fig. 2 (a) Raman spectra of carbon coated Fe NWs that were produced using different CVD temperatures. The intensities were normalized using the 1st order vibration harmonics (G band) as reference. The 1st order vibrational modes were found at 1344 cm^{-1} (D band) and at 1576 cm^{-1} (G band). The 2nd order vibrational modes (overtones) were found around 2689 cm^{-1} (G' band) and around 2929 cm^{-1} (D+G band). (b) Zoomed detail in the 30-55° 2θ region of the XRD patterns of carbon coated Fe NWs at different CVD temperatures. The main diffraction peaks belonging to iron and alumina phases are highlighted, as well as the other detected materials.

Results and discussion

Synthesis and characterization of Fe@C NWs/ AAO nanocomposites obtained at different CVD temperatures

The AAO template used for the fabrication of the nanocomposite is shown in Figure 1(b). The pore size and the thickness of the template after the phosphoric acid treatment was respectively 77 ± 6 nm and 1.67 ± 0.14 µm (Fig. S1). Figures 1(c) and S2b) show SEM images of the obtained carbon-coated Fe NWs after the AAO template removal. The length of the core-multishell NWs was around 1 µm with a diameter of 86 ± 25 nm (Fig. S2), which correlates well with the measured pore size of the templates. In Fig. 1(d), a HRTEM picture shows a conformal carbon coating displaying crystalline graphene layers. The CVD was performed in this case at 750 ºC. The coating was optimized by varying the CVD carbon growth temperature in the range of 600 to 800 ˚C.[8,9] The runs were conducted with an interval of 50 ˚C. Furthemore, a low pressure CVD system was used to maintain a total pressure around 3.31 mbar. To evaluate the quality of the carbon coating that was synthesized at different CVD temperatures, Raman spectra were acquired using a green laser. Fig. 2(a), shows the Raman spectra of the graphite coated Fe NWs after the CVD process. These spectra were recorded after dissolving the AAO template. The resolved G band shows that using the CVD temperatures from 600 ºC to 800 ºC it was possible to grow graphitic carbon on the Fe NWs. The position of this G band (~1580 cm^{-1}) is a signature of sp^2 carbon hybridization which confirms the formation of graphene layers. Alongside with the G band there is also the D band present in our samples (Fig. 2(a)). The D band is common in CVD-grown graphene and is due to structural defects such as the formation of amorphous carbon or sp^3 hybridized carbon. Tipically, the I_D/I_G ratio is used as a measure of the structural quality.[10,11] By

comparing the G band with the D band, we can observe that increasing the CVD carbon growth temperature decreases the number of defects (Fig. 2(a)). Additional information about the structural quality and number of graphene layers can be extracted from the second order harmonic G' band (or 2D). The G' band intensity increases with the CVD temperature, which suggests an increase in the number of layers and a higher quality of the graphene structure around the Fe NWs. Similar Raman behaviour is detected in multiwalled carbon nanotubes (MWCNTs) when increasing the number of layers.[11,12] Low defect graphene layers were achieved at 750 ºC or higher temperature. The results from both D and G' bands agree in that a higher quality graphitic coating was achieved at 800 ºC. This result is also confirmed from XRD (Figs. 2(b) and 4(a)) that shows decreased Fe_3C formation at higher temperatures (peak around 45º). The XRD patterns of Fe NWs embedded in AAO and coated with carbon by CVD at temperatures ranging from 600 ºC to 800 ºC are displayed in Fig. 2(b). The patterns show the presence of α-Fe, C graphite, and some reflections attributed to the cementite phase (Fe_3C), suggesting that carbon diffuses into the body-centered cubic (bcc) structure of Fe to some extent, as observed in other works.[13] The presence of hexagonal graphite is clear at 800 ºC. Besides these phases, other peaks related to the crystallization of amorphous AAO template are detected. Namely, several phases, including γ-, θ- and δ-Al_2O_3 are detected upon increasing the CVD temperature.[14,15] Interestingly, it was noticed that at 800 ºC the AAO template starts to be difficult to etch with 10 wt% NaOH. This can be explained by the transition of alumina to the more stable δ- and θ-Al_2O_3 phases, as shown in Fig. 2(b). Concerning the magnetic properties, the normalized room-temperature hysteresis loops of nanocomposites filled with C-coated Fe NWs at different CVD temperatures are shown in Fig. 3. When the NWs are CVD-treated an inner shell of magnetic Fe_3C is formed. In this case, the overall shape of the loops does not drastically change, in spite of the expected reduction of saturation magnetization (Figs. 3 and S3). A soft-magnetic behaviour with coercivity, H_C, values ranging from 95 to 320 Oe depending on the direction of measurement (along or perpendicular to the NWs axis) and CVD temperature, is encountered. No clear effective magnetic easy axis is observed. This is due to the competition between the magnetic shape anisotropy and the interwire dipolar interactions, as observed in other works.[8,16]

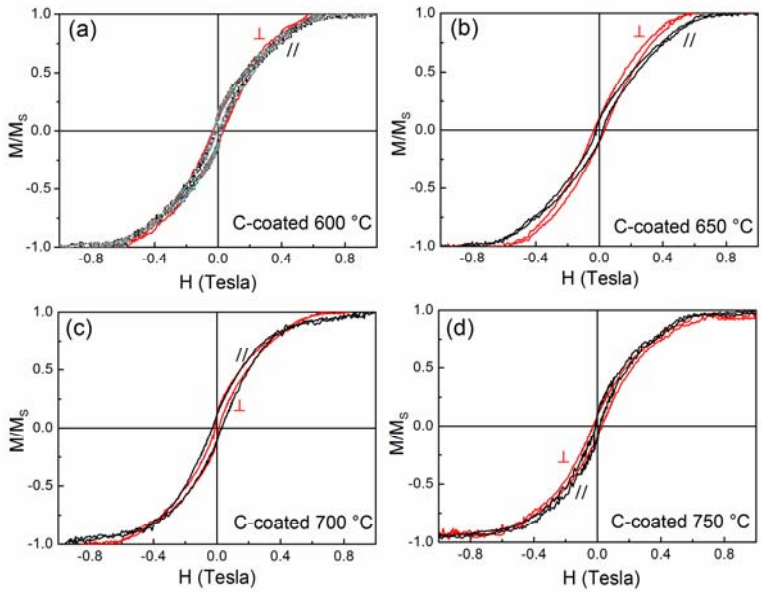

Fig. 3 Normalized room-temperature hysteresis loops of Fe NWs coated with carbon by using different CVD temperatures: (a) 600 ºC, (b) 650 ºC, (c) 700 ºC and (d) 750 ºC. Symbol ∥ means that the field was applied parallel to the NWs axis whereas ⊥ means that the field was applied perpendicular to the NWs axis.

Assessment of the wettability and the biocompatibility of the nanocomposites

During the synthesis of the nanocomposites, the AAO templates become more resistant to chemical etching with increasing temperature. Taking advantage of this phenomenon, magnetic nanocomposites were developed at a higher CVD temperature (900 ºC). The quality of the graphitic multishell structure in the nanocomposite was not evaluated given that the Al_2O_3 from the nanocomposite was not chemically etchable. An SEM image from the nanocomposite after attempting etching is shown in the supporting Figure S4 together with a list of etchants tested. The Al_2O_3 showed a remarkable chemical resistance to both strong acids and bases and a high mechanical resistance to

high power tip sonication.

The structural composition of the nanocomposites was analysed by XRD. From Figure 4(a), we observe that the phases present at 900 ºC are similar to those observed at 800 ºC (cf. Figure 2(b)). The relative intensity of δ- and θ-Al_2O_3 phases are slightly higher, which explains the increase in both chemical resistance and mechanical strength of the nanocomposite.[17,18] In addition, the pattern shows the presence of Fe_3C and C graphite phases, which are absent in the uncoated Fe NWs annealed at 900 ºC. Moreover, Fe oxides/hydroxides are detected in the latter, which further proves that the C coating protects the Fe core from intermixing between Fe and AAO template (i.e., oxygen diffusion).

Further tests were done to characterize the surface properties of the nanocomposite in order to evaluate its suitability for biomedical applications. The surface wettability was determined by the sessile drop method. The contact angle of drops of culture medium on the surface were measured for different fabrication conditions and listed in the supplementary Figure S5. Nanocomposites bearing uncoated Fe NWs (room temperature and annealed at 900 ºC) and others bearing carbon coated Fe NWs (750 ºC and 900 ºC), all displayed hydrophobic behaviour. C-coated samples showed higher contact angles, which corresponds to a higher hydrophobicity. In general, the increase in temperature led to a decrease of the hydrophobic behaviour. Notice that hydrophobicity can be a desirable feature in some biomedical events; e.g. to avoid cells to attach/integrate to an easily removable temporary implant.

Cytotoxicity tests were performed using the WST-1 cell proliferation assay kit. Fibroblasts showed confluence with normal cell morphology after being exposed to culture medium that was incubated with nanocomposites containing either carbon coated or uncoated Fe NWs fabricated at 900 ºC (cf. Materials and Methods). The absorbance measurements showed equal levels of cell proliferation (see supplementary Figure S6) which confirms that toxic ions were not released from the nanocomposite samples at significant levels. This result shows that the nanocomposite is non-cytotoxic. For the case of the carbon-containing nanocomposite, the carbon coating additionally protects the iron from corrosion over time.[18]

Nanocomposite samples were also evaluated in terms of cell adhesion and proliferation on the samples' surface. Samples after different fabrication steps were tested and cell adhesion was observed only on unfilled AAO templates at RT, 750 ºC and 900 ºC (Figures 4(b) and S7). Our experiments show that porous alumina (amorphous and crystalline) is a bioactive material.[19,20] On the other hand, cells did not proliferate on the nanocomposite containing both carbon coated and uncoated Fe NWs fabricated at 750 ºC and 900 ºC. Furthemore, no cells were found on the surface of the filled nanocomposites but still they were proliferating on the well plate around these samples (fig. S8). These results indicate that cells did not adhere to the nanocomposite's surface due to the lack of anchoring points on the nanocomposite and not from cytotoxicity, which is in agreement with the results from the cytotoxicity tests. This also shows that filled nanocomposites are anti-biofouling to fibroblasts.

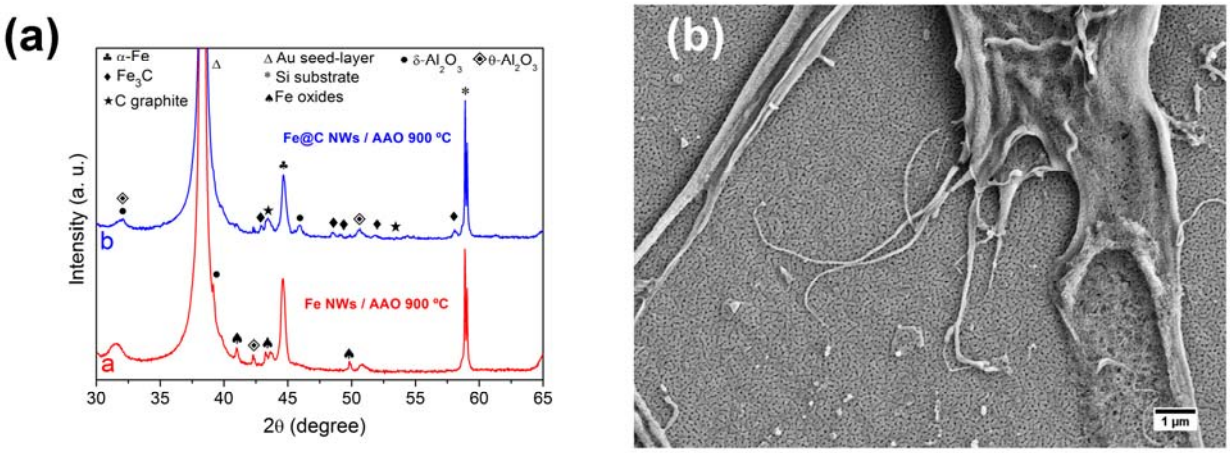

Fig. 4 (a) Comparison of XRD spectra from as-produced nanocomposites filled with uncoated Fe NWs annealed at 900 ºC and C-coated Fe NWs fabricated at 900 ºC. (b) SEM image of fibroblasts proliferating on the AAO template before pore widening at RT. The porous surface is visible in this picture. Fibroblasts grow on the surface of porous unfilled AAO but not on the surface of filled nanocomposites.

Conclusions

In summary, we demonstrate that core-multishell magnetic Fe@C NWs/AAO nanocomposites can be synthesized by template-assisted electrodeposition followed by CVD at 900 ºC. The porous AAO matrix offers a high chemical and mechanical resistance. This has been attributed to the formation of θ- and δ-Al_2O_3 at high temperature. The embedded Fe NWs are covered by very high quality graphitic shells. The carbon quality allows long-term stability of the nanocomposite iron filler over corrosion and provides a framework for reliable linker chemistry. These carbon nanospots can be functionalized to provide anchor points

for cells to adhere, for biosensing or triggered drug release. Magnetic measurements reveal a soft ferromagnetic behaviour in all the investigated samples. The produced nanocomposite is bioinert, non-cytotoxic to fibroblasts and anti-biofouling. We can conclude that by changing the nanostructured surface properties of the material, from porous alumina to filled AAO nanocomposite, one can turn a bioactive material into a bioinert one. The multiple properties of the developed nanocomposite make it a suitable candidate for implementation in several distinct applications. In the field of electronics, it can be used for data storage as magnetic recording media. In medicine, it can be used for electrical or magnetic cell stimulation as an implant or cardiac patch.

Acknowledgements

The authors acknowledge support of the Scientific Center for Optical and Electron Microscopy (ScopeM) and FIRST Center for Micro- and Nanoscience of the Swiss Federal Institute of Technology (ETHZ), as well as the Binnig and Rohrer Nanotechnology Center (BRNC) at IBM Zürich. A.M.L. was supported by Fundação para a Ciência e Tecnologia (grant no. SFRH/BD/51282/2010) through the GABBA PhD program of the University of Porto. E.P. acknowledges the MINECO for the 'Ramón y Cajal' contract (RYC-2012-10839).

Notes and references

[a] *Multi-Scale Robotics Lab, Institute of Robotics and Intelligent Systems, ETH Zurich,8092 Zurich, Switzerland. E-mail: vidalp@ethz.ch.*
[b] *Instituto de Ciências Biomédicas Abel Salazar da Universidade do Porto, 4099-003 Porto, Portugal.*
[c] *Departament de Física, Facultat de Ciències, Universitat Autònoma de Barcelona, Campus UAB, 08193 Bellaterra, Barcelona, Spain. E-mail: Eva.Pellicer@uab.cat.*
[d] *Institució Catalana de Recerca i Estudis Avançats (ICREA), Barcelona, Spain.*

† Electronic Supplementary Information (ESI) available: [details of any supplementary information available should be included here]. See DOI: 10.1039/b000000x/

1 J. Kao, K. Thorkelsson, P. Bai, Z. Zhang, C. Sun and T. Xu, *Nat. Commun.*, 2014, 5, 4053.
2 B. Maxit, D. Bendejacq and V. Ponsinet, *Soft Matter*, 2012, **8**, 1317-1320.
3 L. Liu, W. Lee, Z. Huang, R. Scholz and U. Gösele, *Nanotechnology*, 2008, **19**, 335604.
4 T. V. Thamaraiselvi and S. Rajeswari, *Trends Biomater.* Artif. Organs, 2004, **18**(1), 9-17.
5 D. Brüggemann, *J. of Nanomat.*, 2013, **2013**, 1-18.
6 T. A. Desai, D. J. Hansford, L. Leoni, M. Essenpreis and M. Ferrari, *Bios. & Bioelect.*, 2000, **15**, 453-462.
7 M. A. Zeeshan, K. Shou, S. Pané, E. Pellicer, J. Sort, K. M. Sivaraman, M. D. Baró and B. J. Nelson, *Nanotechnology*, 2011, **22**, 275713.
8 M. A. Zeeshan, S. Pané, S. K. Youn , E. Pellicer, S. Schuerle, J. Sort, S. Fusco, A. M. Lindo, H. G. Park and B. J. Nelson, *Adv. Funct. Mater.*, 2013, **23**, 823−831.
9 J. Deng, P. Ren, D. Deng, L. Yu, F. Yang and X. Bao, *Energy Environ. Sci.*, 2014, **7**, 1919–1923.
10 A. C. Ferrari and D. M. Basko, *Nature Nanotechnol.*, 2013, **8**, 235–246.
11 A. Gupta, G. Chen, P. Joshi, S. Tadigadapa and P. C. Eklund, *Nano Lett.*, 2006, **6**(12), 2667–2673.
12 S.-H. Jeong, H.-Y. Hwang, S.-K. Hwang and K.-H. Lee, *Carbon*, 2004, **42**, 2073–2080.
13 J. Zhu, S. Pallavkar, M. Chen, N. Yerra, Z. Luo, H. A. Colorado, H. Lin, N. Haldolaarachchige, A. Khasanov, T. C. Ho, D. P. Young, S. Wei and Z. Guo, *Chem. Commun.*, 2013, **49**, 258–260.
14 L. Fernández-Romero, J. M. Montero-Moreno, E. Pellicer, F. Peiró, A. Cornet, J. R. Morante, M. Sarret and C. Müller, *Mater. Chem. Phys.*, 2008, **111**, 542–547.
15 M. I. Fernandes Macedo, C. A. Bertran, C. C. Osawa, *J. Mater. Sci.*, 2007, **42**, 2830-2836.
16 J. Escrig, R. Lavín, J. L. Palma, J. C. Denardin, D. Altbir, A. Cortés and H. Gómez, *Nanotechnology*, 2008, **19**, 075713.
17 M. R. Gallas and G. J. Piermarini, *J. Am. Chem. Soc.*, 1994, **77**(11), 2917–2920.
18 T. Van Gestel, C. Vandecasteele, A. Buekenhoudt, C. Dotremont, J. Luyten, R. Leysen, B. Van der Bruggen and G. Maes, *J. Membr. Sci.*, 2002, **207**, 73–89.
19 B. Su, X. He, S. Dhara and J. P. Mansell, *Key Eng. Mater.*, 2007, **330-332**, 975-978.
20 M. Karlsson, E. Pålsgård, P. R. Wilshaw and L. Di Silvio, *Biomaterials*, 2003, **24**, 3039–3046.